Validation and modeling of aeronautical composite structures subjected to combined loadings: The VERTEX project. Part 2: Load envelopes for the assessment of panels with large notches

Joël Serra, Jean-Emmanuel Pierré, Jean-Charles Passieux, Jean-Noël Périé, Christophe Bouvet, Bruno Castanié, Caroline Petiot

▶ **To cite this version:**

Joël Serra, Jean-Emmanuel Pierré, Jean-Charles Passieux, Jean-Noël Périé, Christophe Bouvet, et al.. Validation and modeling of aeronautical composite structures subjected to combined loadings: The VERTEX project. Part 2: Load envelopes for the assessment of panels with large notches. Composite Structures, 2017, 180, pp.550-567. 10.1016/j.compstruct.2017.08.055 . hal-01617966

HAL Id: hal-01617966
https://hal.science/hal-01617966

Submitted on 3 Jul 2018

HAL is a multi-disciplinary open access archive for the deposit and dissemination of scientific research documents, whether they are published or not. The documents may come from teaching and research institutions in France or abroad, or from public or private research centers.

L'archive ouverte pluridisciplinaire **HAL**, est destinée au dépôt et à la diffusion de documents scientifiques de niveau recherche, publiés ou non, émanant des établissements d'enseignement et de recherche français ou étrangers, des laboratoires publics ou privés.

Validation and modeling of aeronautical composite structures subjected to combined loadings: The VERTEX project. Part 2: Load envelopes for the assessment of panels with large notches

Joël Serra [a], J.E. Pierré [a], J.C. Passieux [a], J.N Périé [a], Christophe Bouvet [a], Bruno Castanié [a,*], C. Petiot [b]

[a] Institut Clément Ader (ICA), Université de Toulouse, CNRS UMR 5312-INSA-ISAE-Mines Albi-UPS, Toulouse, France
[b] Airbus Group Innovations, 12 rue Pasteur, 92152 Suresnes, France

A B S T R A C T

One of the important issues in the certification of composite aeronautical structures is large notches. In this paper, tests are carried out on technological specimens under tensile, shear and combined loadings using the VERTEX test rig presented in the first part of this publication. Strong interactions between post-buckling and propagation of cuts are observed. The specifically developed FE-SDIC methodology presented allows a first dialog between calculation and testing. The Discrete Ply Modeling method is able to compute the onset of failure in such complex tests. New test responses called "envelope curves" are proposed and are obtained by following a load path that allows the behavior of the notched structure to be validated for certification purposes. This methodology should eventually lead to a new vision of the test pyramid with the help of "Predictive Virtual Testing" procedures.

Keywords:
Composite structures
Structural testing
Multiaxial loading
Finite element-digital image correlation
Damage
Failure
Model

1. Introduction

The general context of the validation of composite aeronautical structures was recalled in the first part of this article [1]. Certification is still largely based on an experimental, semi-empirical approach called the "pyramid of tests" (Rouchon [2]). This approach is applied to structural sizing in general (common areas, structural details, junctions, etc.), taking into account non-detectable low energy impact damage (below the Barely Visible Impact Damage - BVID) or exceptional damage. In the latter category, aircraft manufacturers must justify their structure under static loads with a large crack that could occur as a result of an exceptional event. Moreover, for certification purposes, this crack must pass through a fuselage frame and is commonly named a "two-bay crack". In general, the certification tests are carried out at full scale with internal pressure as shown in the Airbus test (Fig. 1). As part of aeronautical programs, tests of sandwich panels with large cuts have also been carried out by means of the FASTER Fixture Test [3]. These tests were widely instrumented by a combination of DIC (Digital Image Correlation) analysis, infrared thermography and acoustic emission. They were carried out under various combinations of biaxial tension and internal pressure. The size of the panels was several square meters. Cross-cutting tests were also carried out on PRSEUS type structures on the same system [4].

However, the majority of academic studies on notches are performed at the coupon scale for practical reasons. From an application point of view, due to the complexity of crack tip failure modes, many holes or cracks are sized using point-stress, by calculating the damage at a distance d_0 from the stress concentration [5,6]. For this model, the stress is averaged over this distance d_0, called the "average distance", in order to smooth the stress field in the surroundings of the hole/notch. One of the important issues generated by the study of holes and cracks is the scaling effect [7–12], which can be rendered by "averaged stresses" type models even if the distance d_0 can depend on several factors [6], such as stacking sequence, material, and hole/notch size. The size effect leads, in particular, to a small hole being less penalizing than a large hole (for homothetic size of structures). Numerous experimental and numerical investigations have been conducted in order to explain the physical meaning of the size effect [7–12]. For example, Wisnom et al. [9,10] showed that the strength of notched composite laminates decreased when the notch size increased and concluded that the hole size effect was triggered by the presence of non-critical damage at the ply level, such as fiber failure, ply

* Corresponding author.
E-mail address: bruno.castanie@insa-toulouse.fr (B. Castanié).

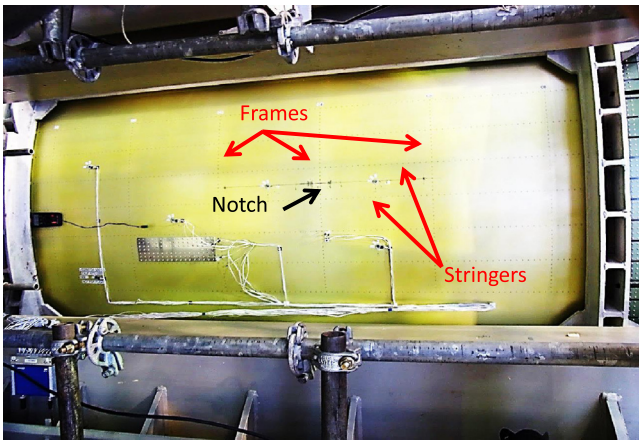

Fig. 1. Typical "Two-bay crack" test (Courtesy of Airbus).

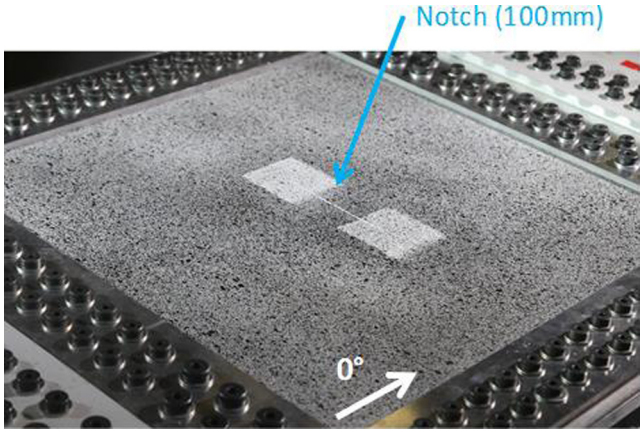

Fig. 3. View of a notched specimen bolted on the test rig.

splitting, delamination or matrix cracking in the vicinity of the hole, smoothing the stress concentration. The ratio of the size of this "fracture process zone" to the specimen size explains the strength difference between small and large specimens. Recently, by using our own modeling strategies known as "DPM" for Discrete Ply Modelling, we succeeded in capturing this size effect on open hole tensile specimens [12] and also on notched specimens [13]. This strategy was initially developed to simulate low energy impact on laminates [14,15] or pull-through [16]. Thanks to its unique capability to capture the failure scenario, the discrete nature of matrix cracking and inter- and intra-laminar damage coupling, this strategy was recently extended to in-plane issues [12,13,17]. In the present paper, this strategy will be extended to the issue of large notches under complex loading and will be recalled only very briefly below.

The VERTEX test method and the FE-SDIC (Finite Element-Stereo Digital Image correlation) measurement strategy have been presented in the first part [1] and are based on the authors' past experience on complex loadings and structural testing [18,19]. Details of the VERTEX collaborative project are given in [20]. Tests carried out on technological specimens and under complex tensile, shear and combined loadings using the VERTEX method are presented in the first part of this paper. A first approach to the calculation/tests dialog on double thickness specimens under tensile and shear loading is then developed. Eventually, new tests called "envelope" tests are proposed and performed. They allow a load path to be followed with the aim of validating the behavior of the notched structure. Prospects regarding research directions and in terms of approaches for the certification of composite structures are also proposed.

2. Materials and methods

2.1. Description of specimens and tests

The stacking sequences were the same as in [12,13]. The plies were made of Hexcel's T700-M21 carbon epoxy unidirectional laminate with a nominal thickness of 0.125 mm. Two specimens were also manufactured with a double thickness ply of 0.250 mm. Three symmetrical stacking sequences of 13 plies were studied. The three different stackings (C3-1, C3-2, C3-3) presented the same number of plies in each direction (0°, 90° and ±45°), and only the relative position of the plies changed between layups:

- C3-1 [45/−45/X/X/X/90/0/90/X/X/X/−45/45]
- C3-2 [X/X/X/X/0/90/0/90/0/X/X/X/X]
- C3-3 [X/X/X/X/X/0/0/0/X/X/X/X/X]

Specimen dimensions were 560 × 540 mm^2 with a central area of interest of 400 × 400 mm^2 [1]. A central crack 100 mm long and 2 mm wide was milled in the center of the specimen [13]. The preliminary test carried out in [1] made it possible to demonstrate that the fasteners sustained the loads without the need for reinforcement plies and therefore the test specimens had a constant

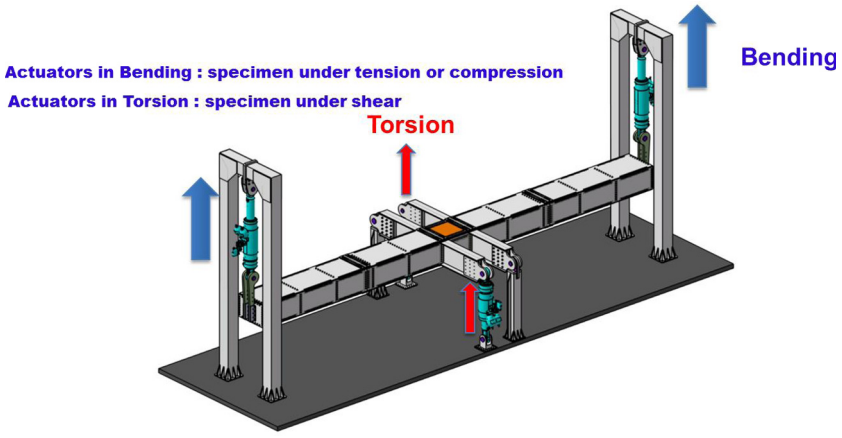

Fig. 2. Vertex test Rig.

Table 1
Tests performed.

	C3-1	C3-2	C3-3
Traction	X + XX	X	X
Shear	X + XX	X	X
Tension + Shear	X	X	X
Envelope Curves	X	X	X

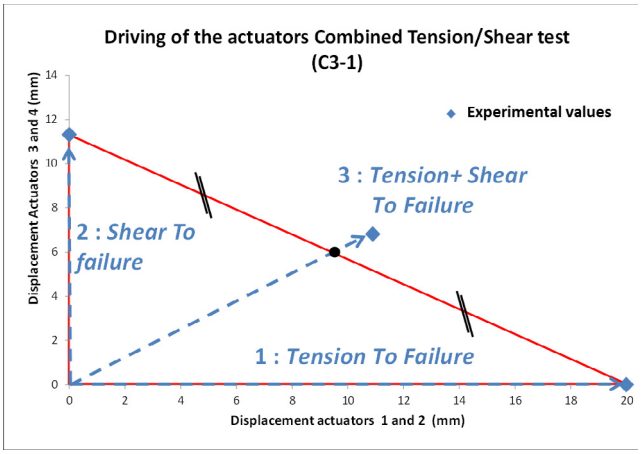

Fig. 4. Combined loading actuators driving policy.

thickness. However, unlike in the preliminary test, aluminum plates were added here to maximize load transfer through friction. The loading principle of the VERTEX assembly is shown in Fig. 2. A view of the test specimen mounted on the VERTEX assembly is shown in Fig. 3.

The list of tests carried out is presented in Table 1. Four tests were carried out for each laminate: tensile, shear, combined and envelope. Two additional tests were carried out on C3-1 with a double thickness ply (0.25 mm instead of 0.125 mm) and were used for the dialog between tests and calculations. These specimens are called "C3-1d". Tensile and shear tests were controlled by imposed displacements as indicated in [1]. For the combined-loads test, the four actuators were driven simultaneously in pairs. Based on the tensile and shear displacements, an average linear loading path was imposed (Fig. 4). The case of envelope loads was more complex and is detailed in Section 5.

2.2. Monitoring strategy

A speckle was printed on the specimens and was digitally defined to optimize the resolution (Fig. 5). For the tests carried out, three pairs of cameras were installed (Fig. 5): a pair of 5 Mpx Pike cameras acquired images of the whole plate (red), a second pair focused on one end of the cut (green) and the third pair, of Prosilica 29 Mpx cameras, acquired images of the entire cut (blue). Given the differences in sensors and lenses used for notch edge

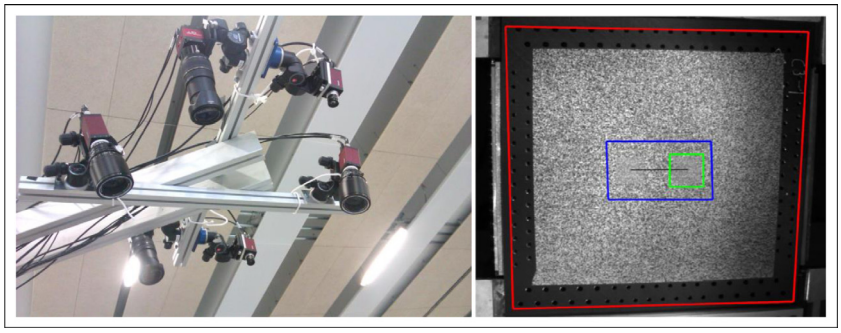

Fig. 5. Set of 6 cameras and areas covered on the specimen.

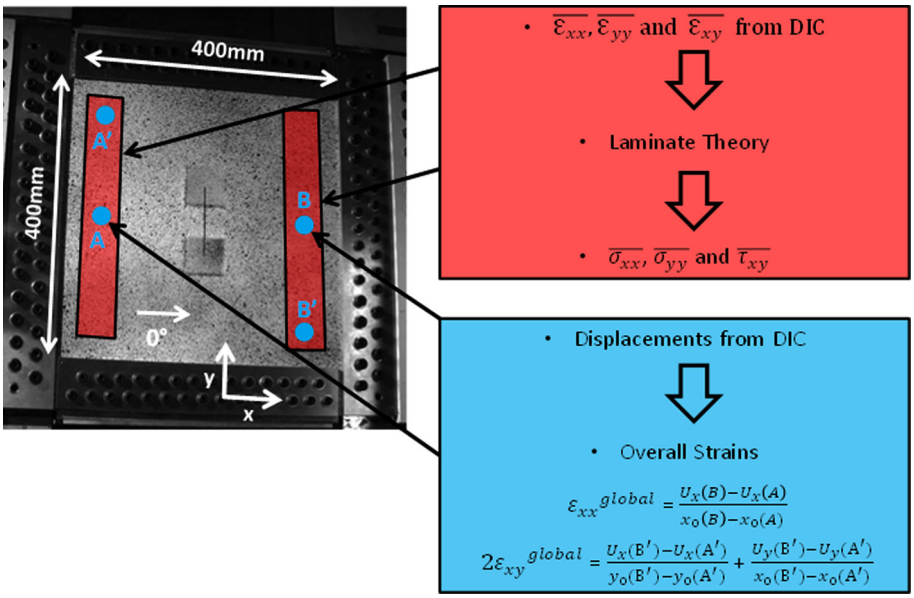

Fig. 6. Tension and Shear Shell Forces in the specimen (Cases 2, 3 and 6, see Table 1).

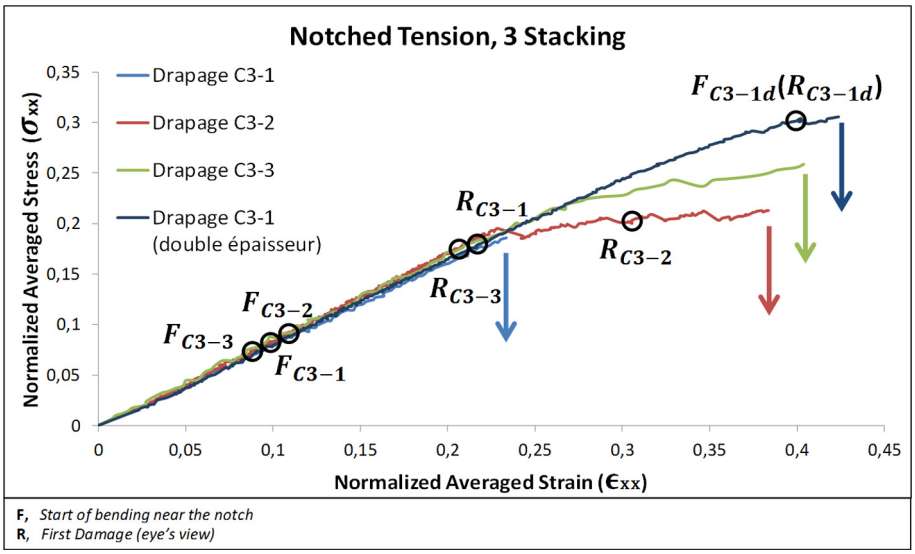

Fig. 7. Notched tension, stress vs strain, averaged and normalized. Four specimens.

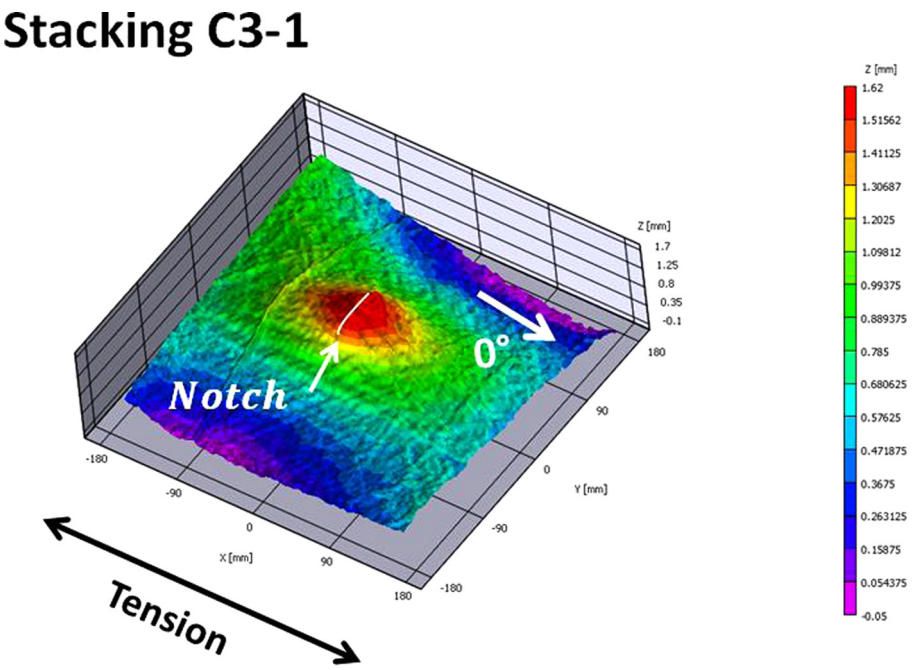

Fig. 8. Local bending (in red) around the notch, Point $F_{C3\text{-}1}$.

measurements, the resolutions of the zones shown in blue and green were approximately the same. The "green" pair therefore merely offers redundancy in the useful measurement for the dialog between the test and the calculation.

As explained in [1] and in [19], the numerous structural redundancies render an *in situ* measurement of the specimen inevitable. The mean stresses were determined by the theory of the laminates from the strains obtained by SDIC (here VIC3D), averaged over the red zones (Fig. 6) at the edge of the zone of interest of the specimen. The parameters used for stereocorrelation are those commonly used. The displacement was measured using subsets of 29×29 px^2. The distance between two consecutive measurements was 7 px. To compute strains, 15×15 displacement measurements were used and the strain was thus estimated using an optical gauge of size $J_v = N_{step}\ (N_{filter} - 1) + N_{subset} = 127$ px. Knowing the resolution of the cameras (5 Mpx), the size of the field of view (350×350 mm^2) and the size of the virtual gauge: 127 px, the surface in the coordinate system of the specimen whose projection corresponds to this virtual gauge was estimated to be 33×33 mm^2. It seems sufficiently small to account for the (small) variation of the gradients in the observed zones (red in Fig. 6). The "global" strains ($\varepsilon_{xx}^{global}$ and $\varepsilon_{xy}^{global}$) were determined by dividing the displacements measured at extreme points (in blue in Fig. 6) by the distance separating them. The imposed shear was calculated in the same way (Fig. 6). The behaviors of the three laminates studied (C3-1, C3-2 and C3-3) were analyzed according to the same methodology for all types of loading: Tension, Shear, Tension/Shear and Envelope. Another method for determining the stress resultants involved in the loading of a specimen by the VERTEX assembly would have been, firstly, to measure the displacement field on

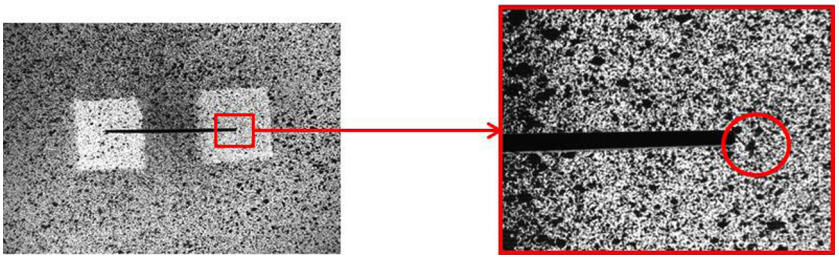

Fig. 9. View of a matrix crack at 45 °for the C3-1 Laminate at point R.

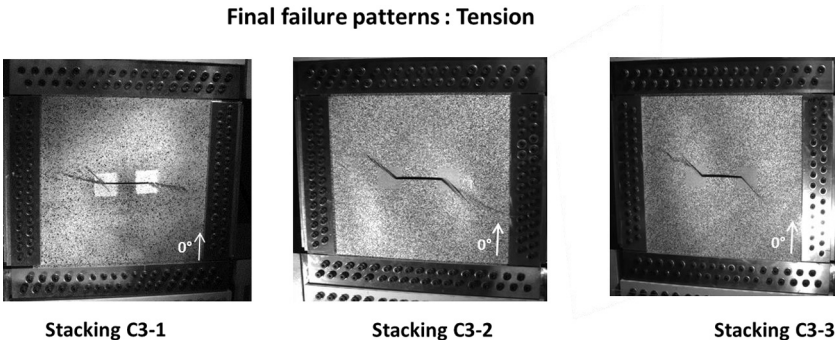

Fig. 10. Final failure patterns (a) C3-1, (b) C3-2, (c) C3-3.

Table 2
Comparison between VERTEX tests and open-hole and notched specimen under tension..

Specimens	C3-1		C3-2		C3-3	
	$\bar{\sigma}^{\infty}$ (%)	CV (%)	$\bar{\sigma}^{\infty}$ (%)	CV (%)	$\bar{\sigma}^{\infty}$ (%)	CV (%)
"Plain"	81	2.5	79	3.7	99	1.5
"Small"	61	4.4	58	1.6	71	9.4
"Medium"	56	1.7	54	4.5	67	0.7
"Large"	53	0.5	50	1.3	57	4.1
"Notched"	38	2.5	41	5.0	40	1.7
"Notched VERTEX"	**19**	**N.A.**	**21**	**N.A.**	**26**	**N.A.**

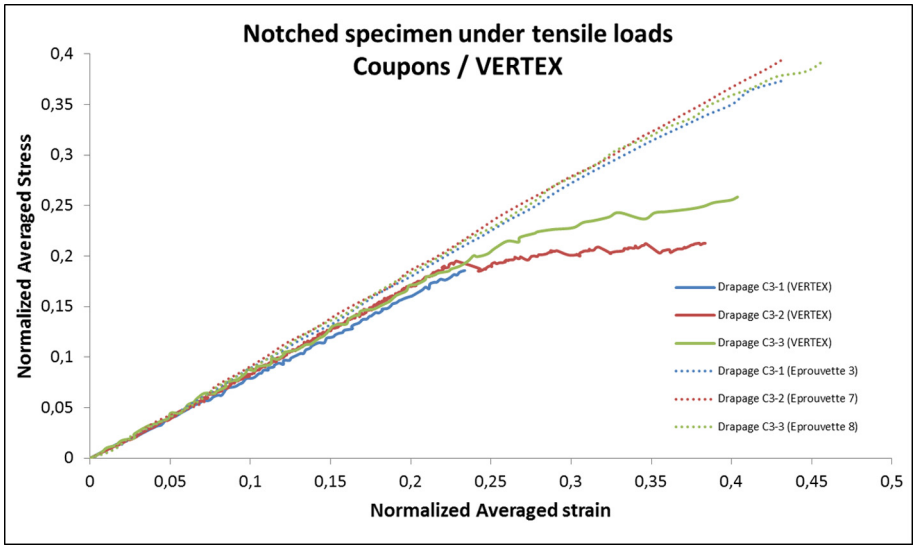

Fig. 11. Comparison between coupon tests and VERTEX tests for notched specimens under tensile load.

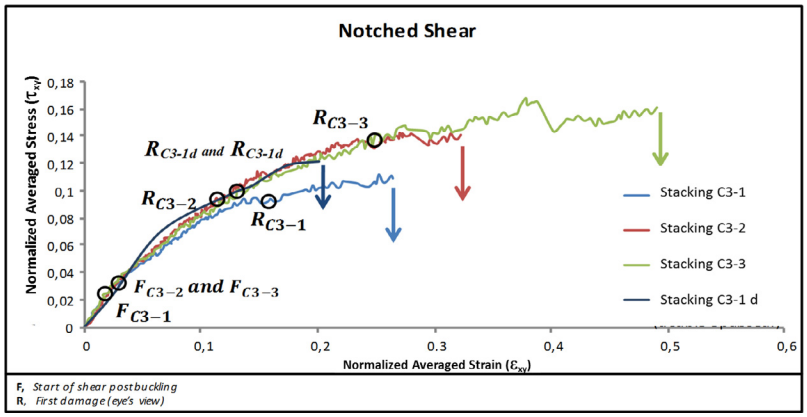

Fig. 12. Notched shear, stress vs strain, averaged and normalized, four specimens.

the edge of the plate by stereocorrelation, secondly, to impose these boundary conditions on a model and, thirdly, to recover the reaction forces associated with each constrained node in motion. After some preliminary tests, this procedure was not implemented in this first phase of the VERTEX studies, mainly because of problems of unresolved border regularization in the FE-SDIC method at that time. The other method described, more robust, was therefore preferred.

3. Tests results and analysis

3.1. Tensile loading tests

Stress/strain curves obtained in tension using the methodology explained in the previous section are shown in Fig. 7. The vertical arrows represent the final failure of the laminates, corresponding to cuts that propagated to the edges of the test piece. The displacement control of the actuators associated with the low acquisition frequency used (1 image/s for the stereocorrelation cameras) generated oscillations on the curves in Fig. 7 and on the others obtained using the same method presented hereafter (Fig. 8 and followings). Using the *in situ* measurement pair (σ_{xx} and ε_{xx}), linear curves were obtained until the damage occurred. In this way, the phases of initial positioning and the possible non-linearities of the assembly were filtered. The specimens were of the same stiffness, 38 GPa, close to the 43 GPa determined experimentally on a notched coupon [13]. This decrease in stiffness was probably due to the ratio of notch width to specimen width, which was higher for VERTEX (1/4) specimens than for coupon-scale (1/6) specimens. This reduction in stiffness was counterbalanced by an increase due to the specific boundary conditions of the VERTEX assembly: the 4 sides of the test piece were clamped, which, by the Poisson effect, theoretically increased its stiffness by approximately 10% ($1/(1-\nu^2)$ with $\nu \approx 0.3$).

Localized bending was observed near the notch (Fig. 8, Layout C3-1). It accelerated the propagation of the crack and thus reduced the maximum failure stress. Points F, indicated by the name of the draping shown in Fig. 7, corresponded to a maximum deflection of the notch border approximately equal to the thickness of the laminate (single thickness: 1.625 mm). The same reference (1.625 mm) was used (in value) for laminates C3-1d. The double thickness laminate, C3-1d, being stiffer in bending, required a higher load to reach similar bending. The failure stress observed for the double thickness specimen was therefore be greater than those observed for the "single thickness". The direction of the local bending observed for the C3-1 laminate (deflecting towards the outside of the box), whatever the thickness of the plate, was not

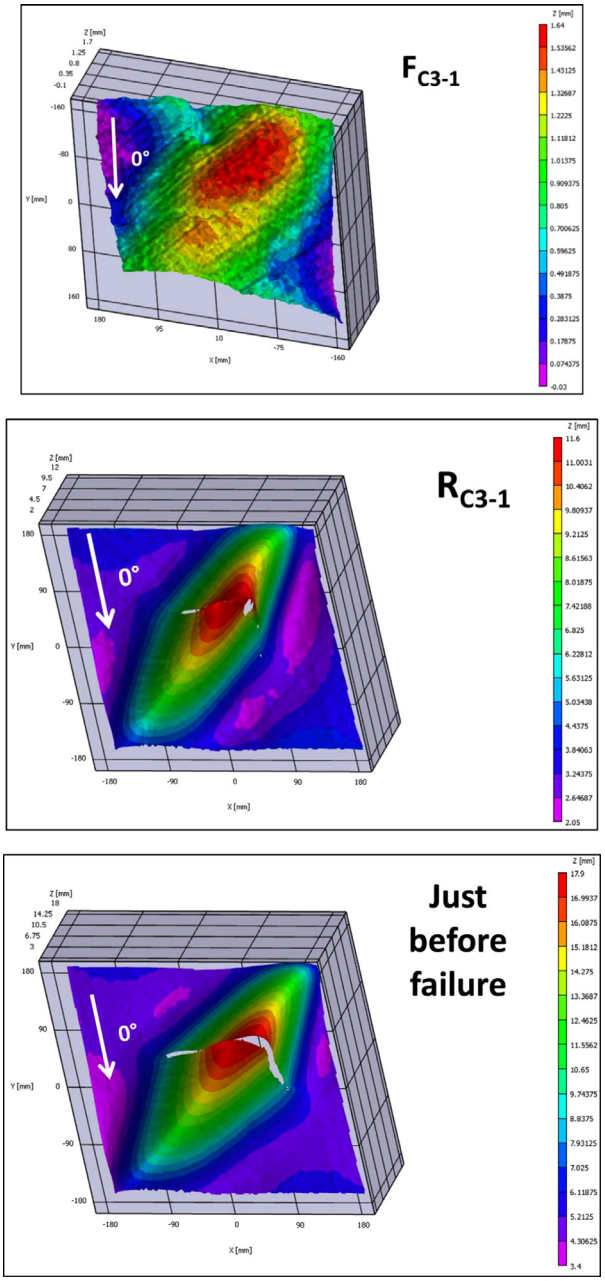

Fig. 13. Out-of-plane displacement field for C3-1 shear test, at points F and R and just before failure.

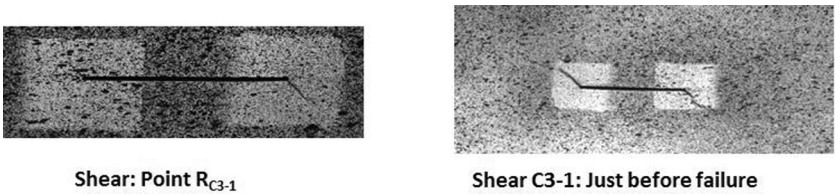

Fig. 14. Cracks visible at the tip of the notch at point R and just before failure.

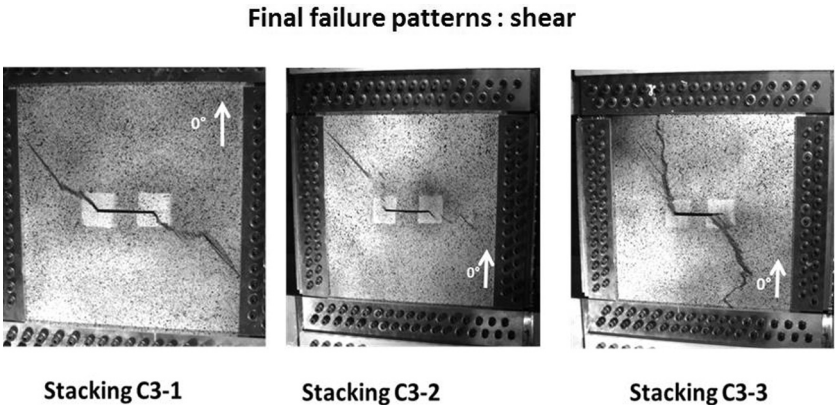

Fig. 15. Final failure patterns for shear tests.

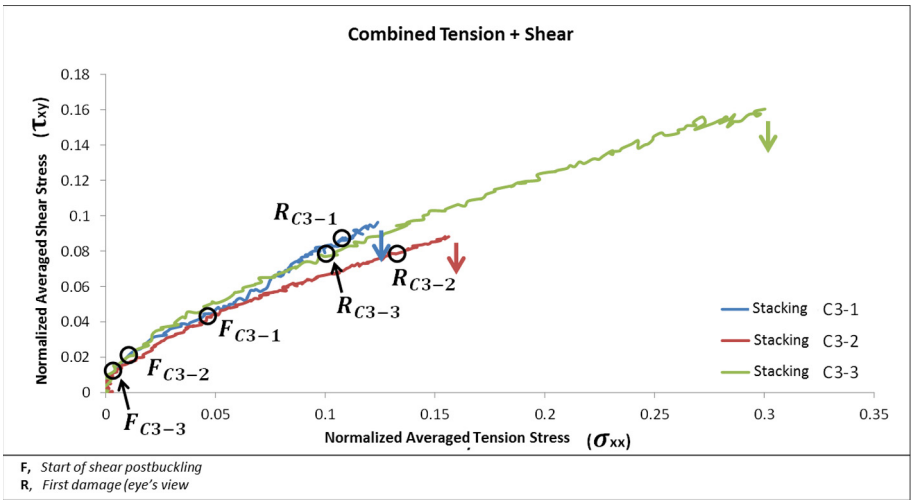

Fig. 16. Notched tension + shear, shear stress vs tension stress, averaged and normalized, three specimens.

Fig. 17. Final failure pattern for combined tension and shear loading.

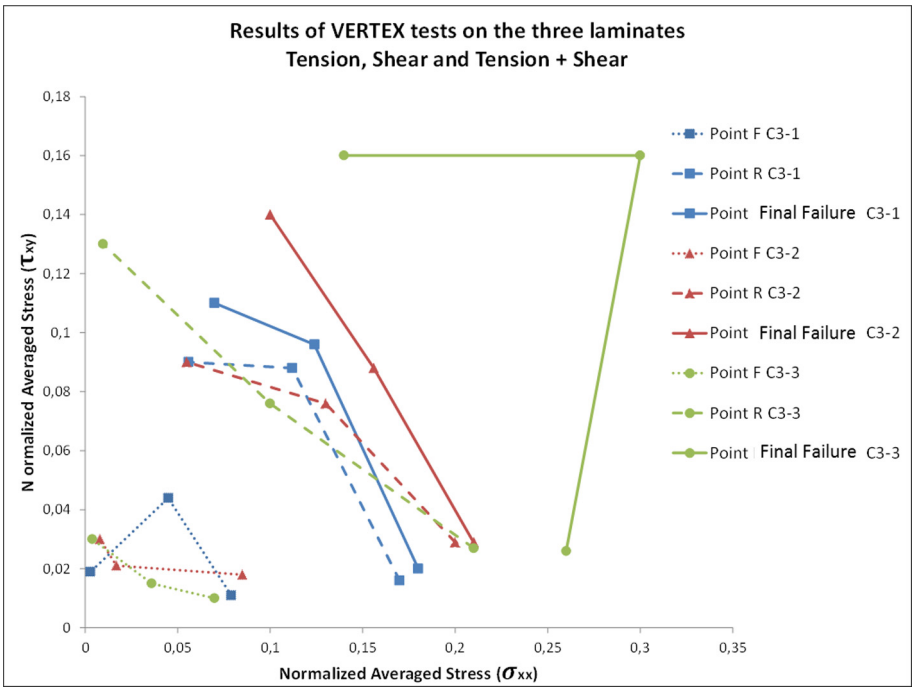

Fig. 18. Summary of the behavior of the three notched laminates under tension, shear and combined loading.

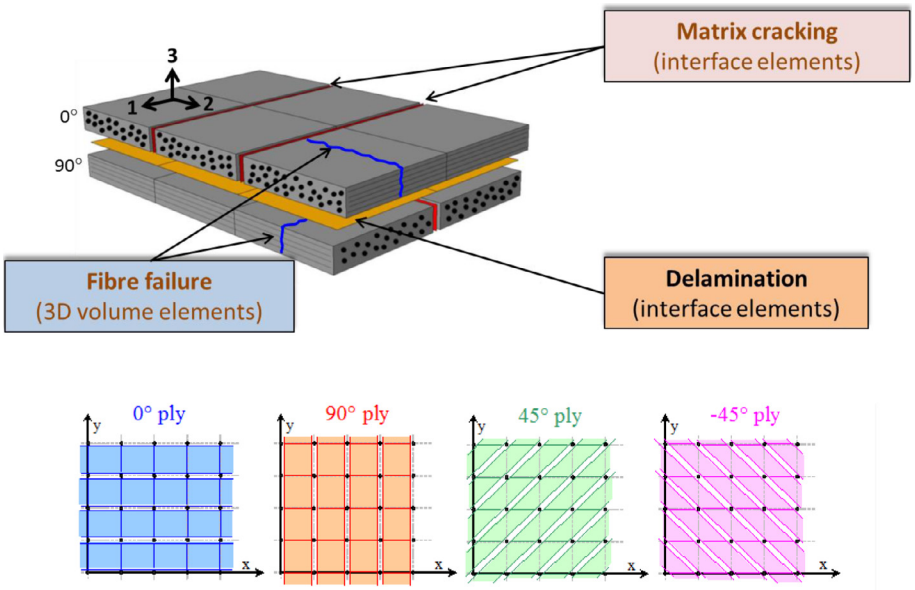

Fig. 19. Discrete ply model main principle and mesh coincidence at interface.

the same as that observed for laminates C3-2 and C3-3 (towards the inside of the loading box). The phenomenon thus seems very unstable and may depend on the initial imperfections of the plate. To verify the latter hypothesis, several tension tests should be carried out on the same laminate and the imperfections measured. It is also possible that this nonlinear geometrical phenomenon was due to the introduction of a local bending moment at the junction between the frame and the upper part of the central box formed by the composite specimen, a problem already identified in [19]. Nevertheless, this behavior was not detected on preliminary tests on aluminum plates [1].

The first failures visually identified are indicated by the points R in Fig. 7. For the C3-1 laminate, the failure was initiated at the notch tip and appeared just before total laminate failure. Cracking of the matrix oriented at 45° on the right side of the notch (Fig. 9), was detected ($\boldsymbol{R}_{C3-1}$). The main difference between the rupture scenario of the VERTEX test specimens and those of the simple test specimens studied in [13] were the influence of boundary conditions. The tension applied in the Vertex test bench is "quasi pure" because the plate is bolted on the 4 sides. Also, the edges of the notch are relatively close to the bolted areas. In this case, the principle of Saint-Venant is not satisfied, and this is what happens in most "structural" tests. Nevertheless, this type of complex test is more representative of the real structures, such as a stiffened fuselage and provides more information than classical tests performed on coupons (Fig. 1).

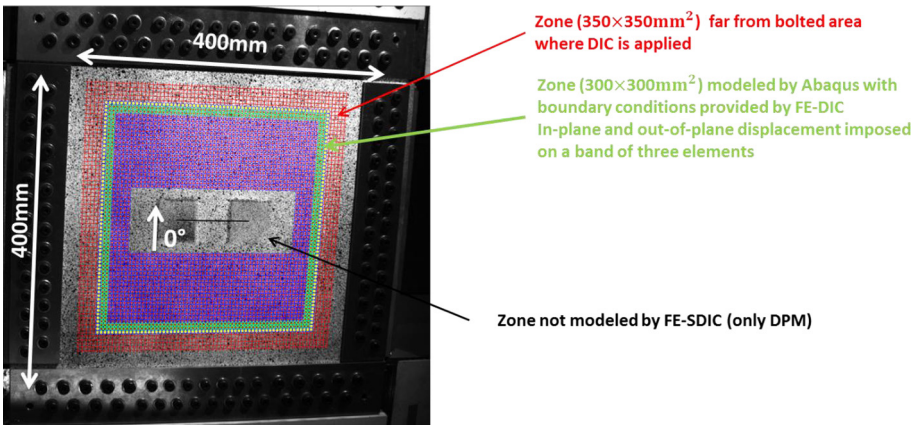

Fig. 20. Method of exchange of boundary conditions between FE-SDIC and numerical model.

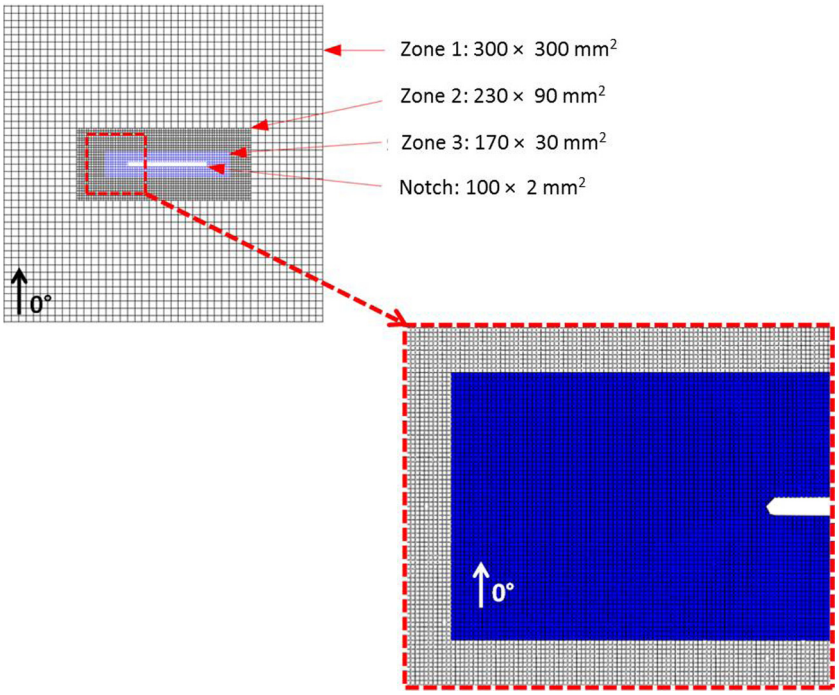

Fig. 21. Abaqus Mesh for analysis of VERTEX tests.

The final failure patterns of the VERTEX specimens are shown in Fig. 10. For laminate C3-1, the pattern is similar to those observed on notched coupons [13]. It resembles a pull-out type with a crack propagation direction inclined at a few degrees from the horizontal. The laminates C3-2 and C3-3 appear to be damaged along different directions: the crack propagates in a direction oriented at 45° and then almost orthogonally to the direction of tension, which is unusual in structural tests [19] but is similar to what is observed in open hole tensile tests [17]. It is interesting to compare the VERTEX tests with the traditional coupon tests carried out in [12,13]. The different tensile stresses for all the tensile specimens studied in this work are summarized in Table 2. The standard test curves are shown in Fig. 11. For the VERTEX tests, we find the following relative order of stresses at failure: $\sigma^{\infty}_{C3-2} \cong \sigma^{\infty}_{C3-1} < \sigma^{\infty}_{C3-3}$. The failure stresses of laminates C3-1 and C3-2 are very close. This confirms that the C3-3 laminate has the best tensile strength, as already observed for the coupons. For the large cut issue, the VERTEX test exhibits structural effects: influence of boundary conditions and probably of initial imperfections of the specimens, which generate localized bending around the notch. These effects produce a significant decrease in the failure strength, which must be taken into account when designing the structure. In addition, the difference between the failure stresses obtained for the "Notched" and the "VERTEX notched" specimens is increased by the difference between the ratios of "failure length to width of the specimen" (respectively 1/6 and 1/4). It also should be noted that the stiffnesses of VERTEX specimens are very similar to those of the "coupon" type specimens (Fig. 11) thus validating the method of determining the stress / strain curves from the DIC.

3.2. Shear loading tests

The shear stress/strain curves are shown in Fig. 12. The vertical arrows represent the final failure of the laminates corresponding to cuts that have propagated to the edges of the test piece. In the same way as in the study of laminates subjected to tension, specific experimental points, noted F, denote a deflection of the edge of the notch here, equal to approximately 1.625 mm, and the points R

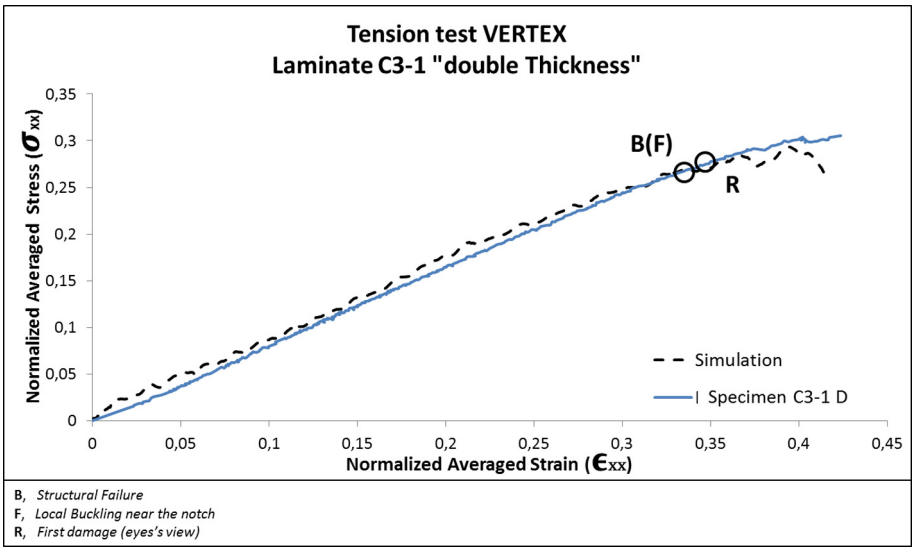

Fig. 22. Experimental/numerical comparison for VERTEX tension test.

Fig. 23. DPM modeling of the first damage (point R).

represent the first damage visually observed (on the surface). Because of the large area of the specimens and their small thickness, the shear buckling occurs quite early and explains the position of points F and the first inflection of the test curves. Buckling occurs a little later in C3-3 and C3-2 than in C3-1 due to the presence of external plies at ±45°. The "double thickness" plate C3-1d logically buckles even later because of its greater stiffness. The shear buckling can be clearly seen at 45° in Fig. 13. From the points R, the behavior of the test pieces shows a strong interaction between the propagation of the cracks and the postbuckling behavior which is very difficult to describe (snap-through). Reference may be made to one of the films of the shear tests (see [21]). As for tension, the first visible damage is a crack at 45° at the notch tip (Fig. 14). The crack propagates slightly but interacts with the postbuckling [21] until sudden final failure. The shear failure patterns for the three laminates are shown in Fig. 15. The failure scenarios and patterns are substantially identical. Crack propagation at 45° is expected in the case of a shear test [19], which is the case for C3-1 and C3-2 – but not for C3-3, where propagation is rather in the 0° direction. This can be explained by the presence of the three 0° plies cluster in the center of the laminate.

3.3. Combined tension/Shear loading tests

The curves of the combined tensile and shear tests are presented in Fig. 16. The vertical arrows here also represent sudden, and loud, propagation of the damage, associated with a significant loss of stiffness. There is a rapid change of slope due to shear buckling despite the presence of a tension stress. The direction of the buckling is, however, deflected with respect to the shear (45°) with a slightly different direction (about 30°). The failure initiations (points R) are very similar to those observed previously except that the cracks at 45° on the surface are not observed here. The film of one of the tests is visible in Ref. [21,22]. The final failure patterns for the three laminates are shown in Fig. 17. The patterns are quite different: for C3-1 and C3-2, the propagation is horizontal, as in pure tension and over practically the entire width of the plate. For C3-3, the failure pattern is completely asymmetrical: the propagation of the crack occurs almost horizontally to the left of the original notch, and is oriented at +45° on the other side. In addition, the combined stress strength of this laminate is much greater than for the other two.

Thanks to the VERTEX tests, it is possible to draw the response of the notched structures under under the three loading conditions. In Fig. 18, the three experimental points recorded for each configuration (laminate/loading) studied are represented: F corresponds to the local bending (or buckling), R to the first damage visually observed on the surface and the total breakage is defined when a first significant decrease in stiffness is observed. The points corresponding to the tensile stresses are the closest to the abscissa axis. Those associated with shear stresses are closest to the ordinate axis. The markers representing the tensile/shear stresses are located between the points mentioned above. The markers are connected by straight line segments to ease understanding. In the case of tensile and shear loading, the uniaxial character of the test degrades as a coupling mode exists in connection with the control displacement driving explained in [1] and the local nonlinear phenomena (postbuckling and local bending). Overall, C3-1 and C3-2 show similar behavior. The crack propagation for C3-3 across the R-points and up to total failure is observed to be much more progressive than for the other two lay-ups. Thus the results on larger samples appear to confirm that the C3-3 laminate has the best resistance, as already noted on the coupon samples subjected to tension [12,13]. In general, at this scale, the different interactions between the various phenomena make it difficult to give simple predictions of the quadratic criterion type.

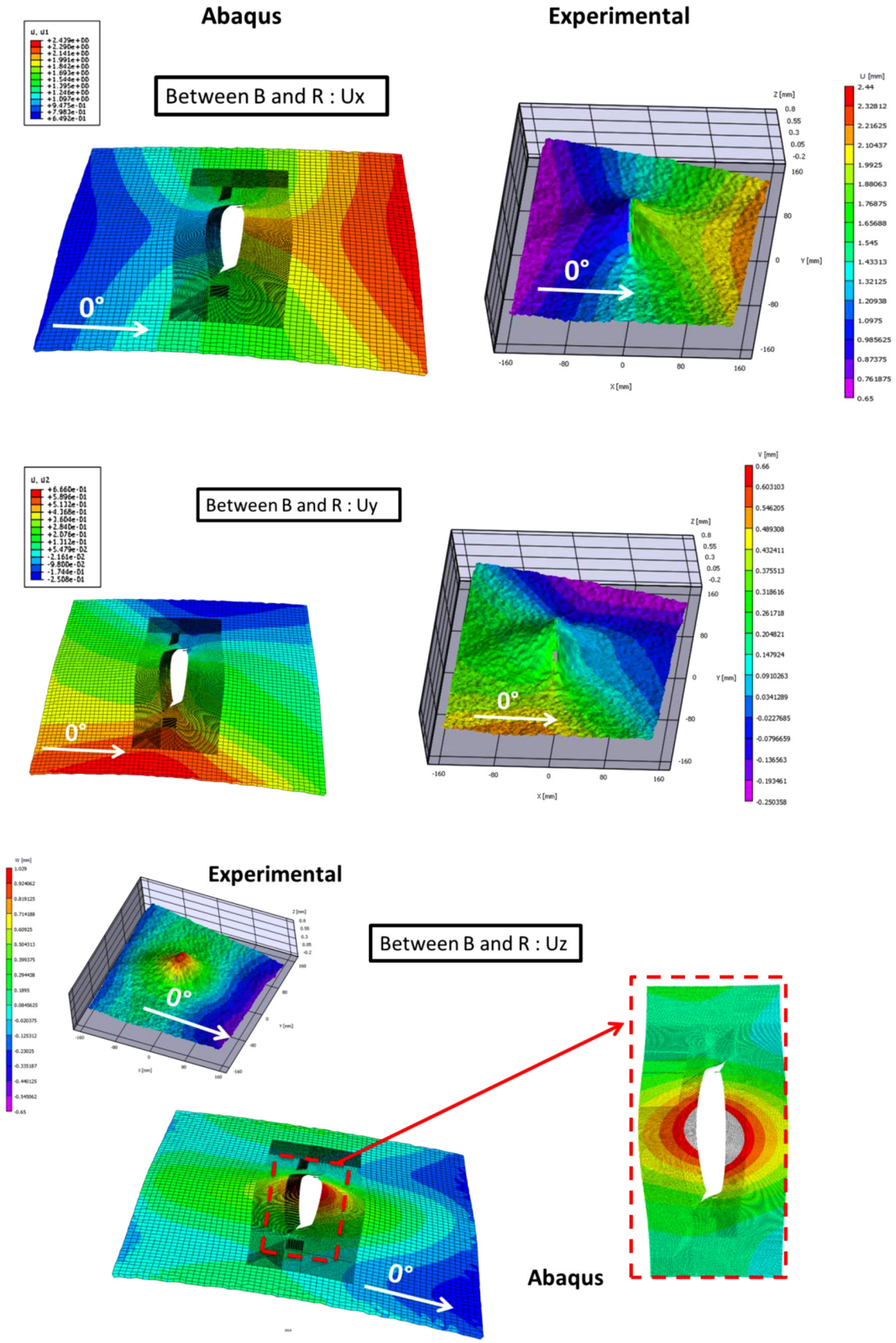

Fig. 24. Comparison of the displacement fields resulting from measurement (DIC) and the numerical model between B and R (W) for maximum tension.

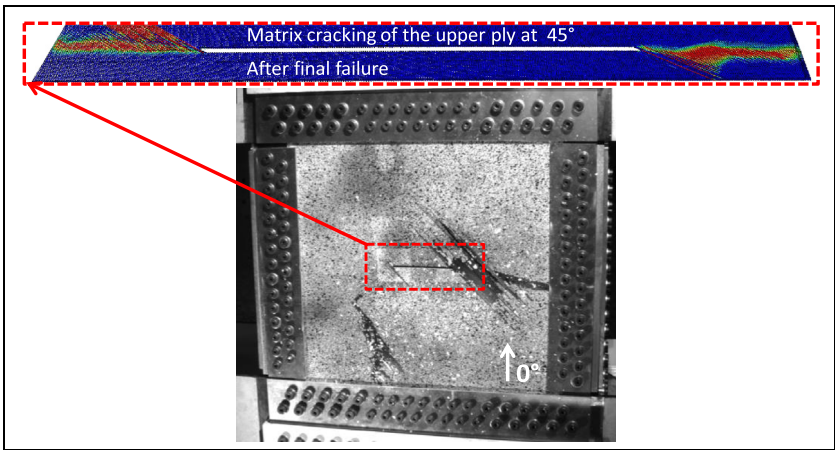

Fig. 25. Failure pattern: numerical vs experiment.

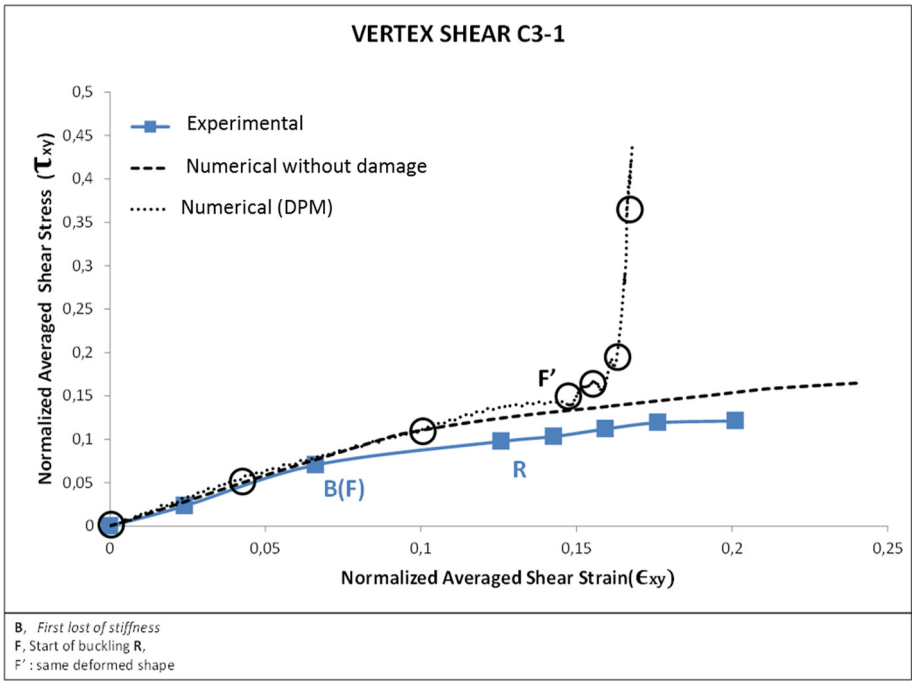

Fig. 26. Stress / strain curves for plate C3-1d, "double thickness" under shear- Numerical / experimental comparison.

4. Modeling of VERTEX tests

4.1. Discrete ply model strategy

The Discrete Ply Model (DPM) has already been described in several papers [12–19] and the same characteristics were kept here as the ones used by Serra et al. for scaled open-hole tension test modeling [12] and notched tensile tests [13]. The main features are briefly recalled below. The principle of the DPM model is to use a dedicated mesh able to represent the discrete character of composite damage like matrix cracking, delamination and naturally, thanks to the geometry of the mesh their coupling (Fig. 19). This approach requires a complex mesh with coincident nodes at the interface (Fig. 19) and a special analysis to mesh holes or notches [12,13,16,17]. The damage laws act as follows:

- The delamination is taken into account using cohesive elements between two consecutive plies (or groups of plies) of different orientation, each ply being modeled with one volumic finite element through the thickness. Then the damage in the delamination interface elements is classically driven by cohesive law with the critical Strain Energy Release Rate (SERR).
- The matrix cracking is taken into account using interface elements normal to the transversal direction. The damage of the matrix cracking interface elements is driven using quadratic Hashin fracture criteria evaluated in the neighboring volumetric finite elements. This interaction is known to be crucial to account for the complex damage morphology observed in composite structures.
- Fiber fracture is taken into account using continuum damage mechanics with an original formulation linking the integration points of the volumetric finite element to impose a constant

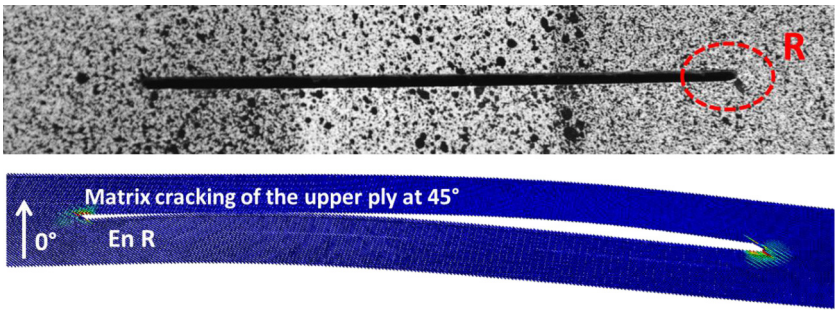

Fig. 27. First damage in the upper ply for double thickness shear test, comparison between experiment and DPM modelling.

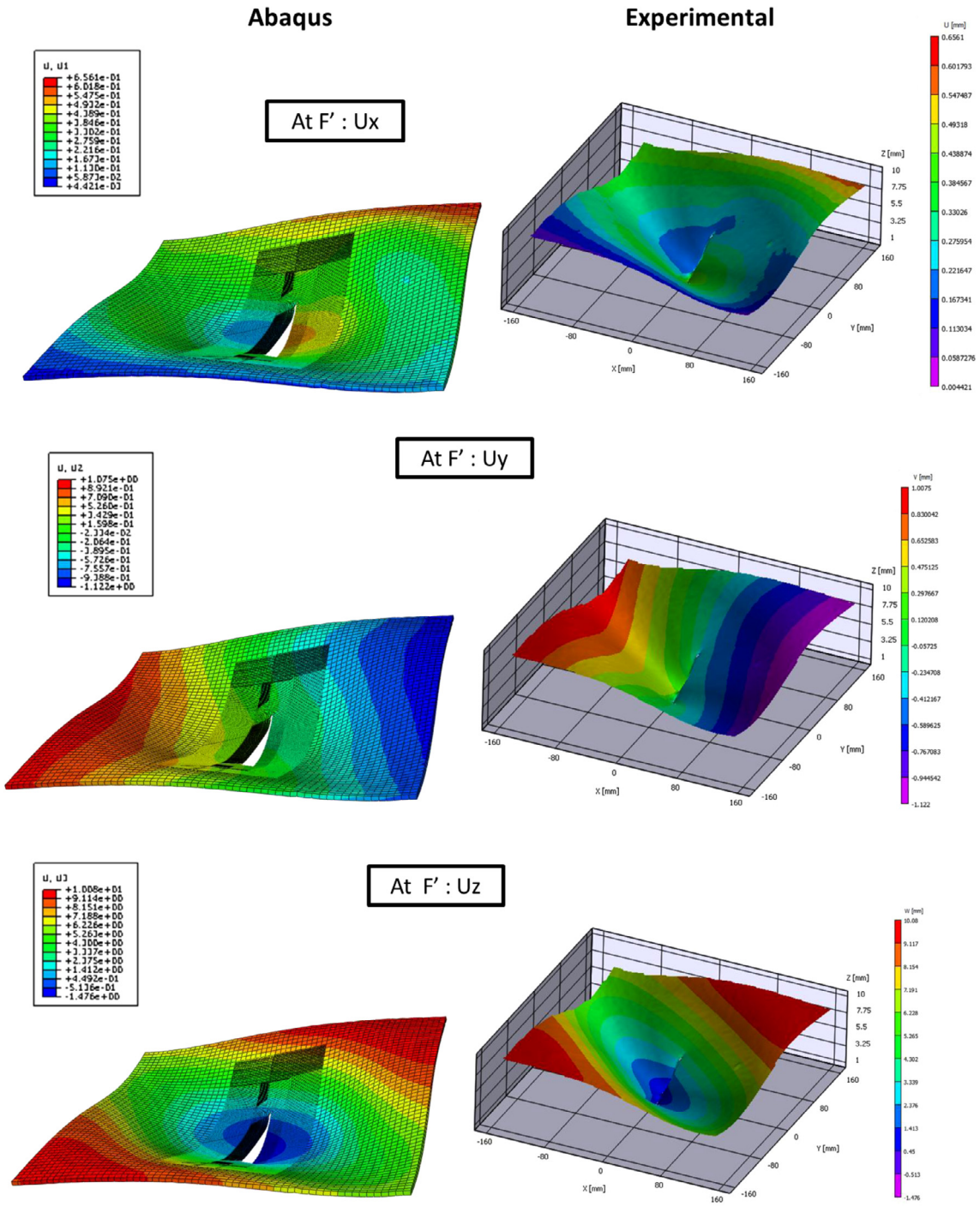

Fig. 28. Displacements at point F′, shear test double thickness, comparison between DPM and test.

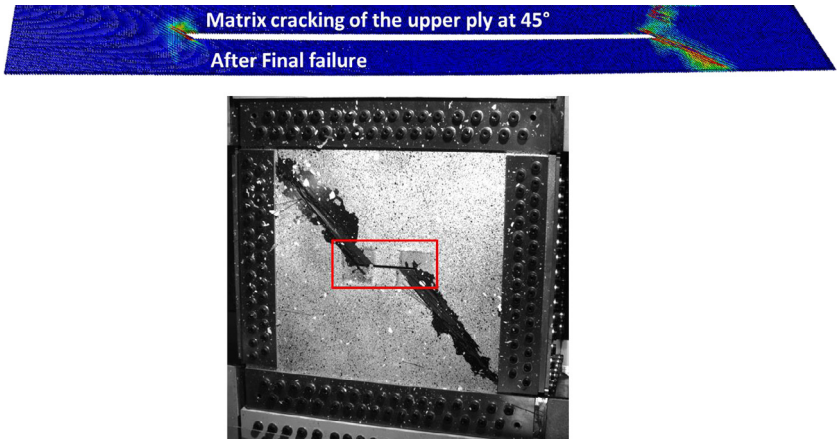

Fig. 29. Final failure for shear test, double thickness, comparison between experimental and numerical result.

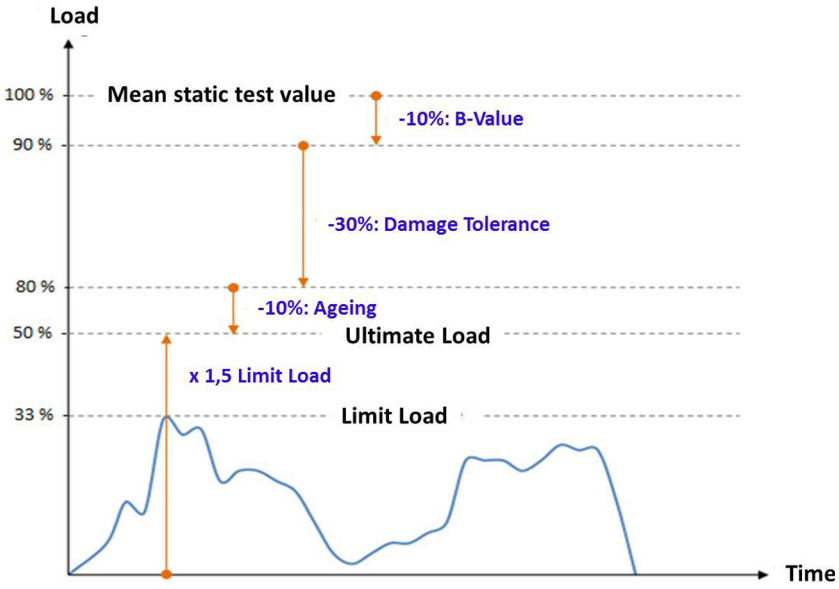

Fig. 30. Qualitative overview of sizing policy for aeronautical composite structure.

SERR per unit area [23]. This approach can be compared to methods using the characteristic element length, which allow mesh-size independent modeling [24–26].

Another strong advantage of this approach is the limited number of parameters, all of which are provided by experimental tests [12,14,16].

4.2. Test/computation dialog

Only the test specimens with double thickness plies C3-1d are modeled here. The general method of data exchange between a finite element model and the FE-SDIC measurements has been explained in the first part of this publication [1] and [27,28]. It gives access to an experimental displacement field directly expressed on the finite element mesh of the model. This avoids complex projections and interpolations between classic DIC and FEA tools. Doing so, experimental displacement-driven simulations are very easy to perform. In the case of the notched composite specimens, it is described in Fig. 20. The measurement is made on the red zone (350×350 mm$^{2)}$, which is smaller than the area of interest (400×400 mm^2) in order to limit edge effects due to bolting. FE-SDIC [27,28] measurements are provided in a 300×300 mm^2 area (where the material is assumed to behave elastically) minus a central rectangle around the notch (in which the evolution of the response can become strongly nonlinear). The boundary conditions are introduced in linear increments as in [1] and following the method described by Sztefek and Olsson [30]. To optimize the computation time, the Abaqus mesh uses three different zones (Fig. 21), generally following the same principle as in [13].

The three components of the displacements measured by FE-SDIC method are first imposed on the edge of zone 1, 300×300 mm^2 (white square, Fig. 20). Then, in order to be able to simulate the rotation better, an out-of-plane displacement is imposed on 3 rows of additional nodes, (green area Fig. 20). In Zone 1 (Fig. 21), the size of the FE-SDIC and Abaqus meshes are identical. The boundary conditions are then simply prescribed dof by dof. The Abaqus mesh is made with SC8 R linear elements with one element in the thickness, size $10 \times 10 \times 3.25$ mm^3. In Zone 2, a mesh is made for each ply with C3D8R linear brick elements. The size of the elements are equal to twice the thickness, i.e. $0.5 \times 0.5 \times 0.25$ mm^3. In Zone 3, at the edge of the crack, the DPM method is applied with C3D8/COH3D8 damaging elements of the same size

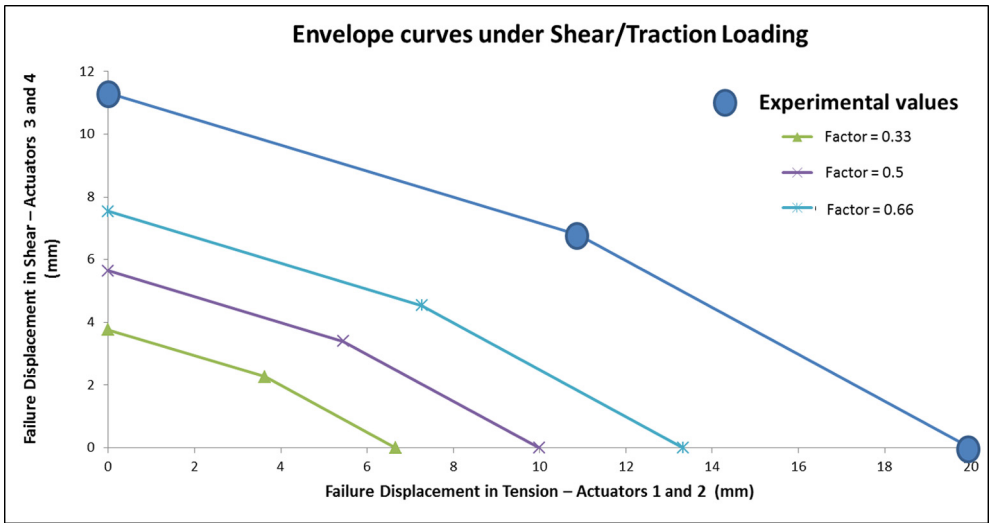

Fig. 31. Loading paths for Envelope Curves.

($0.5 \times 0.5 \times 0.25$ mm^3). In contrast to the modeling of the notched specimens studied at the coupon scale [13], and given the importance of bending/buckling phenomena and the absence of axial symmetry of the boundary conditions imposed, no symmetry is used in the case of the "VERTEX" tests. Therefore, all the 13 plies are modeled. Since DPM imposes the density of the mesh by the thickness of the plies, the number of elements of Zones 2 and 3 is divided by 4 compared to the "single thickness" layups. The calculation takes approximately 4 days (20 CPUs) for a total of 1.7×10^6 elements. For this reason, at this stage, the other tests were not modeled. As in the case of coupons [13], the phenomenon of "shear locking" is not preponderant in this work because the elements located away from the cut use reduced integration (C3D8R and SC8R). However, this type of elements can often lead to poor modeling of bending phenomena because of hourglass modes. To remedy this problem, an artificial energy control of these modes is added to allow the most consistent representation possible. Since this artificial energy is negligible compared to the total internal energy (<1%), the quality of the results is not altered.

4.3. Results

4.3.1. Tensile loading test

The numerically determined stress/strain curve is very similar to the experimental one (Fig. 22). In order to maintain a reasonable calculation time, only 9 of the 44 DIC images used to determine the experimental curve are kept to determine the 8 steps of numerical simulation used. The overall behavior of the laminate appears to be correctly represented. The first surface-detected damage on the composite laminate (R), which is similar to that shown in Fig. 9, is well transcribed by the numerical model (Fig. 23), which correctly simulates matrix cracks oriented at 45° at the notch tip. A comparison with the observed displacement field (Fig. 24) shows that the DPM gives a very accurate simulation of the behavior observed experimentally, in particular the initiation of local bending around the notch. Fig. 25 compares the numerical and experimental failure patterns. On the right side of the specimen, the propagation of damage seems to occur initially in a direction oriented at 45° and then horizontally (orthogonal to the direction of tension). A similar scenario is obtained using the numerical model.

4.3.2. Shear loading test

A first computation was made without introducing any damage, in order to verify that the postbuckling response was correctly captured, and then a second DPM computation was performed. Fig. 26 shows that the numerically determined stress/strain curve is very similar to the curve determined experimentally up to point F in the case of the shear test. Despite the fact that the experimental and numerical constraint curves are close, the numerical buckling is symmetrical to the real situation at the beginning of the computation and then shifts to the real solution after a certain time, with or without simulated damage. This shows that the method for introducing the displacements chosen can still be enhanced, especially through better consideration of initial imperfections and rotations, which is crucial for good modeling of postbuckling phenomena. Nevertheless, the DPM model correctly identifies the initiation of damage observed at point R (Fig. 27), deformed shapes at point F′ (Fig. 28) and the failure pattern (Fig. 29). However, a divergence in the sense of a probable stiffness increase of numerical origin appears in the explicit DPM calculation beyond the point F′.

5. Envelope curves

The certification of composite structures is based on the pyramid of tests (see the first part of this paper [1]) and essentially on uniaxial tests brought to total failure. The general sizing of aeronautical composite structures in civil aircraft is complex and depends on the areas considered [29–32]. Generally speaking, the basic principles of sizing are postbuckling, damage tolerance, and repair and material issues: aging and material scatter (A and B values). In addition, the limit loads (LL) represent the maximum flying loads that an aircraft can handle (hard landing, avoidance maneuvers), for which the aircraft must be sized in fatigue, and ultimate loads (UL), the static limit loads multiplied by a factor of 1.5. The cumulative knockdown factors are represented in an empirical and qualitative way in Fig. 30. The blue curve is taken to represent the profile of the stresses during a flight. For a given problem, it can therefore be estimated that current composite structures will not exceed 33% of their average static failure value for limit loads and 50% for extreme loads. This shows both the margin of progression of composites in aeronautics and the robustness of current structures. For example, some aeronautical structures have demonstrated their ability, with impact and manufacturing defects in pristine condition, to withstand 3 times the lifetime in flight, and then withstand an extreme load to finally satisfy a crash test. The idea of envelope curves is that, in order to validate the sizing of an area or to answer a given problem (large notches, impact damage), it is possible to perform a load path using the VERTEX

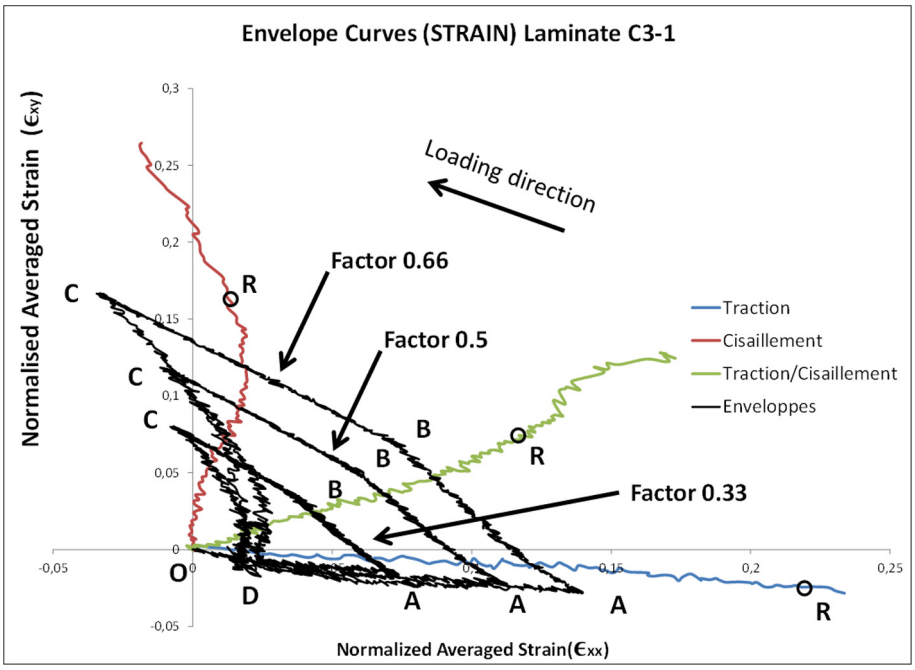

Fig. 32. Envelope tests in the strain space.

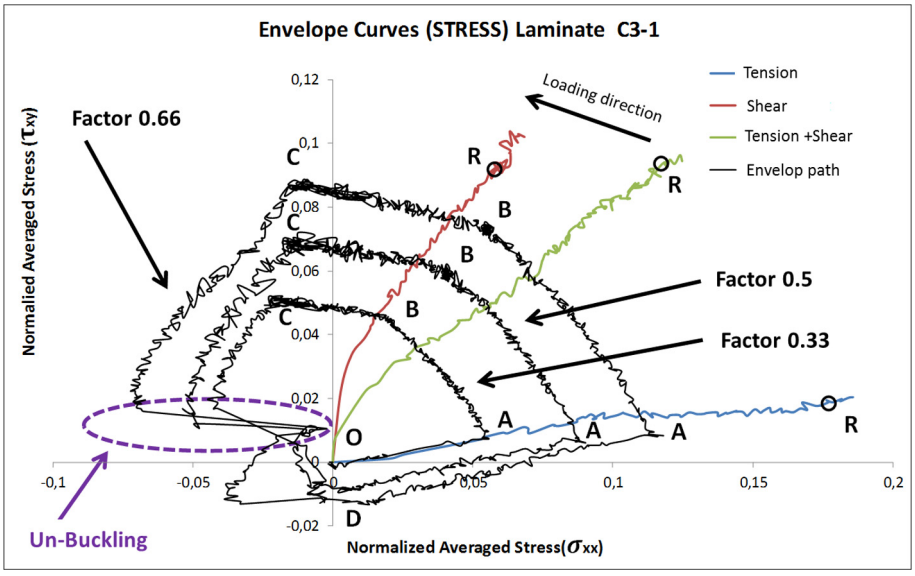

Fig. 33. Envelope tests in the stress space.

methodology at a percentage of the first failure load (R Points) for which the structure remains undamaged. In our case, the percentages used are 0.33, 0.5 and 0.66 and the results for the C3-1 laminate will be presented here. The loading path required by the test results is bilinear (Fig. 31). At this stage of the development of VERTEX, the path will be determined from the displacements of the jacks obtained for the first failures.

The results of the envelope tests are presented in Fig. 32 in a strain space and Fig. 33 in a stress space. These two figures show the behavior of the envelopes performed for the different coefficients (0.33, 0.5 and 0.66) and those of the previous tests (Tensile, Shear, Tensile/Shear) for the C3-1 laminate. The continuous cycle corresponds to: O-A-B-C-D-A-B-C-D-A-B-C-D. The points associated with the first damage to the surface (R) visually observed are shown on the three test curves (Tensile, Shear, Tensile/Shear). In Fig. 31, the segments drawn represent the load displacement paths of the actuators of the Vertex machine. These figures show the influence of the nature of the structural tests and of the "blind" control by the displacement of the actuators at this stage of the use of the VERTEX methodology. The average stresses and strains are not pure because of secondary strains or stresses. A sudden unbuckling is at the origin of the strong discontinuities observed during the paths C → D. It is important to note that a state of stress (or strain) is influenced by the "path" followed to establish it. For the coefficient 0.33, the points A of the envelope curves are very close to the tensile curves while the points B and C are respectively distant from the curves of tension/shear and shear. These deviations between the points obtained by non-proportional loading

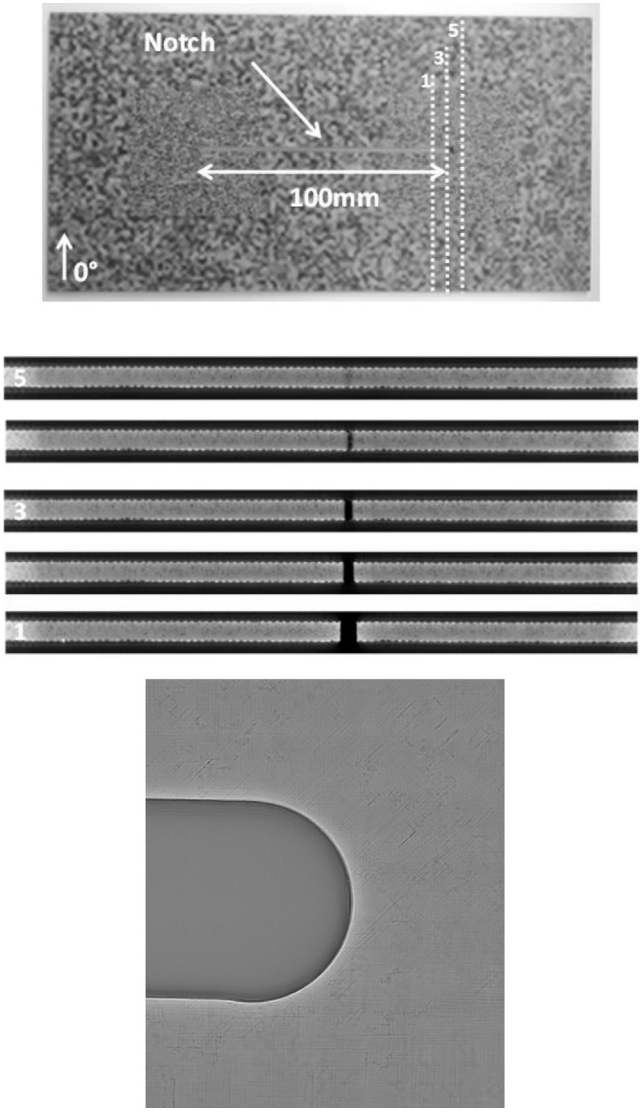

Fig. 34. Micro tomographic sections revealing no damage around the tip of the notch.

Table 3
Material properties of the T700/M21 used in the Discrete Ply Model.

Elastic Properties		
E_1^T	Tensile Young's modulus in fiber direction	130 GPa
E_1^C	Compressive Young's modulus in fiber direction	100 GPa
E_2	Transverse Young's modulus	7.7 GPa
ν_{12}	Poisson ratio	0.3
G_{12}	Shear modulus	5.0 GPa
Matrix cracking		
Y^T	Transverse tensile strength	60 MPa
S^L	In-plane shear strength	110 MPa
Fiber failure		
ε_0^T (%)	Tensile strain in fiber direction at damage initiation	1.70%
ε_0^C (%)	Compressive strain in fiber direction at damage initiation	1.25%
$G_{Ic}^{fibre,t}$	Fracture toughness for mode I in tension	100 N/mm
$G_{Ic}^{fibre,c}$	Fracture toughness for mode I in compression	20 N/mm
Delamination		
G_{Ic}^{del}	Interface fracture toughness for opening mode (I)	0.5 N/mm
$G_{II,c}^{del}$	Interface fracture toughness for shear mode (II & III)	1.6 N/mm

and those obtained by proportional loading are accentuated when the coefficients 0.5 and 0.66 are used. It is clear that, because of the nonlinear nature of postbuckling, the loading path alters the behavior of the structure (buckling and unbuckling). The objective was nevertheless achieved, that is to say part of the Tension-Shear domain was swept in a single test on a notched specimen. X-ray tomography (Fig. 34) confirmed the absence of damage. The sample was shown to be healthy for all cases of extreme loads in the Tension-Shear range, and even beyond, as shown by the use of the factor 0.66.

6. Conclusions and perspectives

In these two papers, a methodology for testing composite structures under complex loadings has been developed. A specific test device for performing tensile/compression, shear and internal pressure tests has been designed, tested and validated. This type of test requires both control and monitoring of the resultant loadings applied to the specimen under test. Thus, a specific full-field measurement method based on a finite element approach to stereo

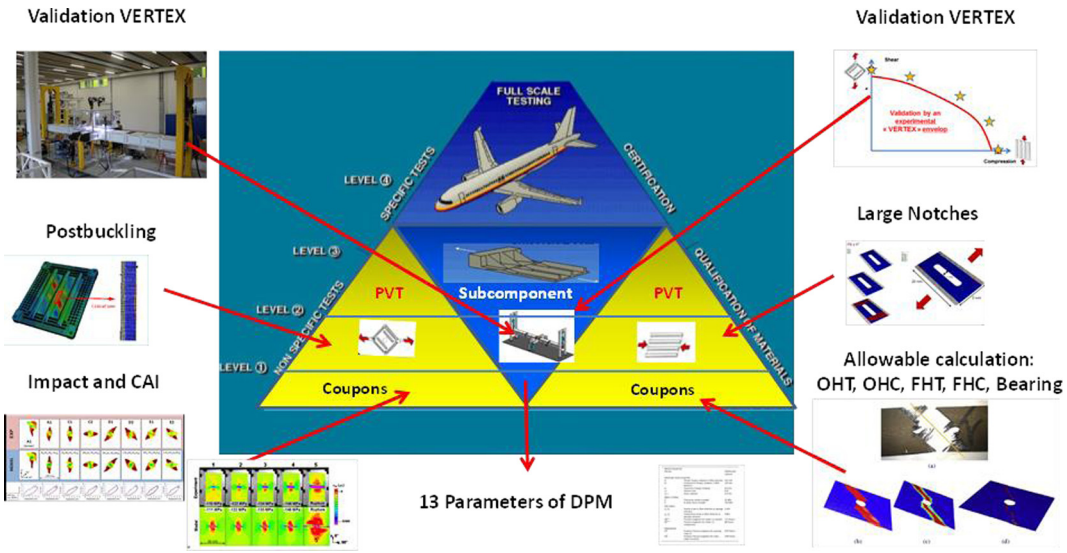

Fig. 35. Perspective for VERTEX: new pyramid of tests with more Predictive Virtual Testing.

image correlation (FE-SDIC) has been developed. The measurement mesh is shared with the finite element model, making data exchanges much easier. A specific protocol has been created and allows for effective and direct test/computation communications between simulated and experimental quantities. This methodology was then applied to the large cuts issue. The experiments revealed very complex behavior with coupling between postbuckling and crack propagation. DPM modeling was then used to successfully predict the first damage and crack propagation onset. The very long computation times (4 days) have allowed only two tests to be modeled for the moment, with plies 0.25 mm thick. Efforts therefore need to be made in terms of optimization of computation time and the damage model. A concept of envelope curves has also been presented. By means of a suitable load path, it enables validation of the structure integrity by means of a swept zone. At this stage, the boundaries of the domain are the experimental results obtained in tensile, shear and combined loadings. The next step will be to compute these boundaries numerically by the DPM method or by the VERTEX partners' approaches [24–26]. In the long term, certification of structures should evolve towards even more *Predictive Virtual Testing* (Fig. 35). The VERTEX approach and the principles of envelope test methodology open the way towards multiple perspectives leading to savings in cost and lead time in the certification process for aeronautical products. They contribute to perspectives of savings in testing, especially at expensive subcomponent and component levels, and to the de-risking at lower pyramid scale level, earlier in the process and at cheaper price, of design principles by intensive usage of numerical predictions supported by a smaller number of test validations. The contribution of VERTEX should ultimately lead to a significant reduction in the number of design loops and the cost of certification of aeronautical structures (Table 3).

Acknowledgments

The research that led to the results presented above received funds from the French National Research Agency under the VERTEX project MATETPRO program (ANR – 12 – RMNP-0001).The academic authors gratefully acknowledge the support provided by Airbus Group Innovation. The test rig was funded by Region Occitanie through a CPER 2010-2014 grant. The authors also wish to thank Sogeclair Aerospace for their work as the contractor on the design and manufacture of the test rig.

References

[1] Serra J, Pierré JE, Passieux JC, Périé JN, Bouvet C, Castanié B. Validation of aeronautical composite structures under multiaxial loading: the VERTEX Project. Part 1: Experimental Setup, Instrumentation with FE-SDIC and Procedures, Composite Structures (in revision).
[2] Rouchon J. Certification of large airplane composite structures, recent progress and new trends in compliance philosophy. ICAS 1990;2:1439–47.
[3] Leone FA, Bakuckas JG, Shyprykevich P, Davies C. Structural testing and analysis of honeycomb sandwich composite fuselage panels November 2008. DOT/FAA/AR-08/51.
[4] Bergan A, Bakuckas JG, Lovejoy A, Jegley D, Linton K, Korkosz G, Awerbuch J, Tan TM. Full-scale test and analysis of a PRSEUS fuselage panel to assess damage-containment features. In: 2011 Aircraft airworthiness & sustainment conference, San Diego, California, April 18–21.
[5] Awerbuch J, Madhukar MS. Notched strength of composite laminates: predictions and experiments – a review. J Reinf Plast Comp 1985;4(1):3–159.
[6] Tan SC. Stress concentrations in laminated composites. CRC Press, Taylor and Francis Group; 1994.
[7] Bazant ZP. The scaling of structural strength. London: HPS; 2002.
[8] Bazant ZP, Daniel IM, Li Z. Size effect and fracture characteristics of composite laminates. J Eng Mater Technol 1996;118(3):317–24.
[9] Wisnom MR, Hallett SR, Soutis C. Scaling effects in notched composites. J Comp Mat 2010;44(2):195–210.
[10] Xu X, Wisnom MR, Mahadik Y, Hallett SR. An experimental investigation into size effects in quasi-isotropic carbon/epoxy laminates with sharp and blunt notches. Comp Sci Tech 2014;100:220–7.
[11] Camanho PP, Maimí P, Dávila CG. Prediction of size effects in notched laminates using continuum damage mechanics. Comp Sci Tech 2007;67(13):2715–27.
[12] Serra J, Bouvet C, Castanié B, Petiot C. Scaling effect in notched composites: the Discrete Ply Model approach. Comp Struct 2016;148:127–43.
[13] Serra J, Bouvet C, Castanié B, Petiot C. Experimental and numerical analysis of CFRP notched coupons under tensile loading. Submitted to Composite Structures.
[14] Bouvet C, Castanié B, Bizeul M, Barrau JJ. Low velocity impact modelling in laminate composite panels with discrete interface elements. Int J Sol Struct 2009;46(14-15):2809–21.
[15] Rivallant S, Bouvet C, Hongkarnjanakul N. Failure analysis of CFRP laminates subjected to compression after impact: FE simulation using discrete interface elements. Comp Part A 2013;55:83–93.
[16] Adam L, Bouvet C, Castanié B, Daidié A, Bonhomme E. Discrete ply model of circular pull-through test of fasteners in laminates. Comp Struct 2012;94(10):3082–91.
[17] Achard V, Bouvet C, Castanié B, Chirol C. Discrete ply modelling of open hole tensile tests. Compos Struct 2014;113:369–81.
[18] Castanié B, Barrau JJ, Jaouen JP. Theoretical and experimental analysis of asymmetric sandwich structures. Comp Struct 2002;55(3):295–306.
[19] Castanié B, Barrau JJ, Jaouen JP, Rivallant S. Combined shear/compression structural testing of asymmetric sandwich structures. Exp Mech 2004;44(5):461–72.
[20] http://www.institut-clement-ader.org/vertex/.
[21] Vertex Shear Test: https://www.youtube.com/watch?v=G5nbiq3b7OA.
[22] Vertex Tension + Shear Test: https://www.youtube.com/watch?v=45AgoMu3fXs.
[23] Ostré B, Bouvet C, Minot C, Aboissière J. Edge impact modeling on stiffened composite structures. Comp Struct 2015;126:314–28.
[24] Abisset E, Daghia F, Ladevèze P. On the validation of a damage mesomodel for laminated composites by means of open-hole tensile tests on quasi-isotropic laminates. Comp Part A 2011;42(10):1515–24.
[25] Marcin L, Maire JF, Carrère N, Martin E. Development of a macroscopic damage model for woven ceramic matrix composites. Int J Dam Mech 2011;20(6):939–57.
[26] Laurin F, Carrere N, Huchette C, Maire JF. A multiscale hybrid approach for damage and final failure predictions of composite structures. J Comp Mat 2013;47(20–21):2713–47.
[27] Pierré JE, Passieux JC, Périé JN. Finite element stereo digital image correlation: framework and mechanical regularization. Exp Mech 2017;53(7):443–56.
[28] Pierré JE, Passieux JC, Périé JN, Bugarin F, Robert L. Unstructured Finite Element-based Digital Image Correlation with enhanced management of quadrature and lens distortions. Opt Lasers Eng 2016;77:44–53.
[29] Niu MCY. Composite airframe structures. Hong Kong: Hong-Kong Conmilit Press; 1992.
[30] Zagainov GL, Lozino-lozinsky GE, Composite materials in aerospace design, Chapman and Hall London; 1996.
[31] Kassapouglou C. Design and analysis of composite structures. Wiley; 2010.
[32] Abrate S, Castanié B. Rajapakse YDS. Dynamic Failure of Composite and sandwich structures. Springer; 2013.